engineering proceedings

MDPI

Proceeding Paper

A Hybrid Propulsion-Based Mission Architecture for the Removal of Debris from Low-Earth Orbit †

Sasi Kiran Palateerdham [1,2,*], Abdul Rahman [1], Emiliano Ortore [1] and Antonella Ingenito [1,*]

[1] School of Aerospace Engineering, Sapienza University of Rome, Via Salaria, 851, 00138 Roma, Italy; abdulrahman.xxx@uniroma1.it (A.R.); emiliano.ortore@uniroma1.it (E.O.)
[2] Italspazio srl, Via della Madonnina, 20A, 95030 Catania, Italy
* Correspondence: sasikiran.palateerdham@uniroma1.it (S.K.P.); antonella.ingenito@uniroma1.it (A.I.)
† Presented at the 14th EASN International Conference on "Innovation in Aviation & Space towards sustainability today & tomorrow", Thessaloniki, Greece, 8–11 October 2024.

Abstract: Satellite technology has advanced with rising demand from the service sector, but increased accessibility also raises risks to the orbital environment. Space debris in low-Earth orbit (LEO) poses a major threat to satellite operations and access to space. Potential solutions for debris removal include using an onboard propulsion module to deorbit a satellite or employing a robotic arm on a "chaser" satellite to capture and remove debris. This study examines active debris removal from LEO at 2000 km altitude, focusing on a target debris weight of 100 kg and a chaser-satellite mass of 100 kg. The mission's velocity change was calculated using the Hohmann transfer for different trajectories, and propellant requirements were derived using Tsiolkovsky's rocket equation: $\Delta V = Isp \times g0 \times \ln(mf/mi)$. Several scenarios were considered to assess the mission's feasibility with respect to debris removal.

Keywords: space debris; active removal method; hybrid rocket; mission design

check for updates

Academic Editors: Spiros Pantelakis, Andreas Strohmayer and Nikolaos Michailidis

Published: 7 March 2025

Citation: Palateerdham, S.K.; Rahman, A.; Ortore, E.; Ingenito, A. A Hybrid Propulsion-Based Mission Architecture for the Removal of Debris from Low-Earth Orbit. *Eng. Proc.* **2025**, *90*, 4. https://doi.org/10.3390/engproc2025090004

Copyright: © 2025 by the authors. Licensee MDPI, Basel, Switzerland. This article is an open access article distributed under the terms and conditions of the Creative Commons Attribution (CC BY) license (https://creativecommons.org/licenses/by/4.0/).

1. Introduction

Advancements in space technology have led to a steady increase in the number of artificial satellites utilized for applications like telecommunications, navigation, and remote sensing [1]. Microsatellite research has further boosted satellite launches from various end users [2]. However, once missions are completed, defunct satellites and rocket components remain in orbit for centuries, posing collision risks to active satellites [3–5]. This growing space debris threat increases the likelihood of collisions, contributing to the debris belt [6]. Kessler's 1978 theory predicted this issue, one which could degrade the space environment and hinder future space applications [7,8].

Following Kessler's seminar, key publications, including the American Institute of Aeronautics and Astronautics (AIAA) paper on debris, in 1981 [9], as well as the ESA Space Debris Working Group [10], UNCOPUOS Technical Report on Space Debris [11], and International Academy of Astronautics (IAA) position paper on orbital debris (2001) [12], led to the formation of the Inter-Agency Space Debris Coordination Committee (IADC) [13]. The IADC, a global forum for coordinating space debris activities, implemented mitigation techniques endorsed by the United Nations. These strategies focus on reducing space debris generation across a mission's lifecycle, including design, operation, and disposal. Passive debris removal methods are used during mission phases, while remediation efforts target current debris, primarily in low-Earth orbit (LEO) and geosynchronous regions, through active removal methods [14,15].

Several studies have been conducted investigating active debris removal (ADR) methods using a mothership, known as chaser, that can be orbited into the required orbital altitude, and considered the possibility of detumbling the targeted debris and allowing it to further deorbit [16,17]. Udrea and Nayak (2015) studied a multi-satellite mission aiming to control debris in low-Earth orbit [18], while Nishida et al. investigated a micro-satellite system using electro-dynamic tether (EDT) technology [19]. Castronuovo [20], Tadini et al. [21], and DeLuca et al. [15] explored the use of chemical rocket systems for deorbiting. This paper focuses on mission design strategies using a Hohmann transfer and a hybrid rocket propulsion system for small satellites; these act as chasers to capture and de-orbit debris in a cost-effective and sustainable manner, ensuring the long-term safety of Earth's orbital environment.

2. Mission Definition

This study presents a case analysis of debris located in a circular orbit at an altitude of 2000 ± 5 km, which serves as the target orbit. A circular orbit at an initial altitude of 500 km is designated as the starting platform for the mothership. A potential case requiring an out-of-plane maneuver is also considered by varying the plane inclination from 5 to 45 degrees. The mothership ascends to the target orbit using velocity changes enabled by a hybrid rocket engine. The engine configuration incorporates nitrogen oxide as the oxidizer, which is chosen for its self-pressurizing properties, and an HTPB-based propellant as the fuel, selected for its proven performance, long-standing reliability, and moderate regression rate. The chaser with the hybrid rocket travels to the debris at an altitude of 2000 km, where it docks with the debris using a mechanical system such as a robotic arm. Later, the mechanism operates to detumble the debris and Hybrid rocket to transfer it back to the base orbital plane.

2.1. Design of Trajectory

The Hohmann transfer trajectory minimizes the total change in velocity (ΔV) required for an orbital transfer between two coplanar circular orbits, utilizing the radius of the initial orbit (R_i) as the periapsis and the radius of the target orbit (R_f) as the apoapsis, following an elliptical orbital transfer path. The ΔV of a Hohmann transfer for co-planar orbits can be defined, as in Equation (1):

$$\Delta V = \Delta V_1 + \Delta V_2 = \sqrt{\frac{\mu}{R_o}}\left(\sqrt{\frac{2R_f}{R_f + R_i}} - 1\right) + \sqrt{\frac{\mu}{R_f}}\left(1 - \sqrt{\frac{2R_i}{R_f + R_i}}\right) \quad (1)$$

If we consider a relative inclination (Δi) between the transfer orbital planes, the variation of inclination Δi is achieved by an out-of-plane maneuver.

In this case, the magnitude of ΔV can be calculated, using the law of cosines, from the known v and θ. Or, more simply, we can divide the isosceles triangle into two right triangles, as shown at the right of Figure 1, and directly obtain ΔV, as in Equation (2), for the circular orbits.

$$\Delta V = 2V \operatorname{Sin} \frac{\Delta V}{2} \quad (2)$$

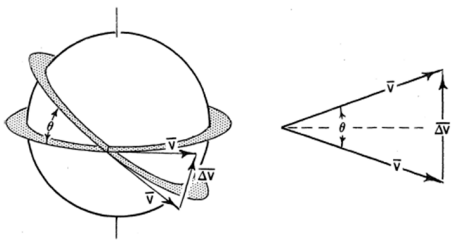


Figure 1. Simple plane change through an angle θ (image credit: Reference [22]).

2.2. Design and Sizing of Hybrid Rocket Engine

A hybrid rocket engine is designed for a given change in velocity (ΔV). Given this low DV, and consequent low thrust requirement, the pressure in the combustion chamber was set to 20 bar.

The specific impulse (Isp), O/F ratio, and thrust coefficient (CF) for the chosen nozzle expansion ratio (e) have been calculated using the NASA chemical equilibrium code.

The sizings of the fuel grain, nozzle, oxidizer tank, injector plate, and combustion chamber casing were performed using the data from CEA and the equations for hybrid rocket engine design from Srivastava et al. [23,24] The initial input conditions from NASA CEA are given in Table 1. The burning time was assumed to be 10 s.

Table 1. Initial conditions for hybrid rocket design.

I_{sp}	Force	T_b	P_c	O/F	a	n	Gamma
290	120	10	20	4	0.178	0.5	1.13

The mass of the propellent is calculated as given in Equations (3) and (4):

$$\dot{m}_p = \frac{F}{I_{sp} g_0} \tag{3}$$

$$\dot{m}_f = \frac{\dot{m}_p}{1 + OF} \tag{4}$$

The combustion chamber was designed according to Equation (5), in light of Mariotte's formula. This equation determines the thickness of the casing as a function of the internal pressure (P), internal radius (r), maximum allowable tension of the material (σ), and the safety factor (n_s). The chamber's length is defined by summing the length of the grain, pre-combustion chamber, post-combustion chamber, and catalytic pack length for the ignition procedure.

$$t = \frac{n_s P_r}{\sigma} \tag{5}$$

The orifice diameter of the injector is calculated using Equation (6):

$$A_{ori} = \frac{\dot{m}_{ox}}{n.C_d\sqrt{2\rho_{ox}\Delta P}} \tag{6}$$

The solid grain is made from HTPB with a single port. The initial port radius is calculated from the mass flow rate of the oxidizer. The final radius is calculated with Equation (7):

$$R(t) = \left(a(2n+1)\left(\frac{\dot{m}_{ox}}{\pi N}\right)^n t + R_i^{2n+1} \right)^{\frac{1}{2n+1}} \tag{7}$$

The lengths of the pre-combustion chamber and post-combustion chamber present are another important factor for hybrid rocket engine based on N_2O as oxidizer. The precombustion chamber allows for N_2O decomposition while the post combustion chamber allows maximum combustion based on pyrolysis. The corresponding pre- and post-combustion chamber lengths can be given as $0.5D_{int}$ and $0.7\ D_{int}$.

As for the oxidizer tank design, a hemispherical cylindrical shape was assumed. Since N_2O is sensitive to changes in temperature, a safety coefficient of 3 was considered. The ullage volume is 5% of the total tank volume. The equation for the radius of the tank is given as Equation (8):

$$f(R) = R^3.\left(\frac{4}{3}\pi\right) + R^2.(\pi.L) - V_{ox} \tag{8}$$

A convergent–divergent nozzle was designed based on the nozzle expansion ratio and thrust coefficient obtained from the NASA CEA code. The lengths of the convergent and divergent sections are

defined by the α and β angles respectively. The throat diameter can be obtained from the relation given in Equation (9):

$$A_t = \frac{T}{CF.P_c} \quad (9)$$

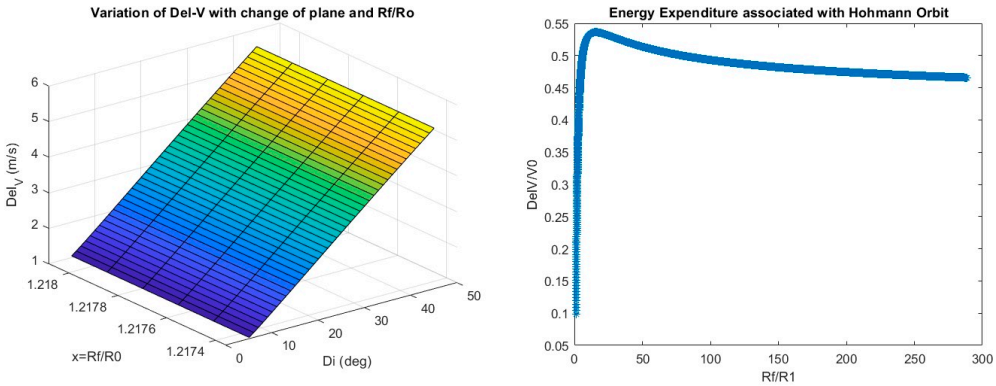
And the corresponding exit area can be calculated from Equation (10):

$$A_e = A_t.e \quad (10)$$

3. Results and Discussion

3.1. Change in Velocity for the Mission

A Matlab code was developed for the given trajectory using the equations from Section 2.1. The results were plotted, as shown in Figure 2. It can be noted from Figure 2a that the change in velocity increases with increases in Δi and increases in the ratio of R_f/Ri. The Δv required to perform a Hohmann transfer between two circular orbits is not at its greatest when the destination radius is infinite. The Δv required is greatest (53.0% of smaller orbital speed) when the radius of the larger orbit is 15.5817 times that of the smaller orbit. The calculated ΔV/V0 is less than that of the maximum range, as shown in Figure 2b.



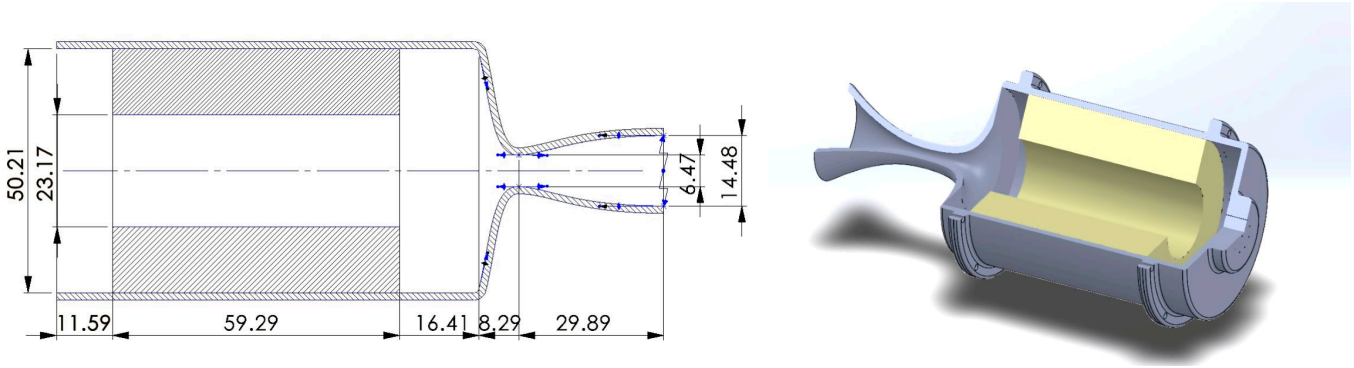
(**a**) (**b**)

Figure 2. (**a**) Variation of Del_V with the change of plane angle and R_f/R_0; (**b**) the corresponding energy expenditure in the Hohmann transfer.

3.2. Numerical Results for the Hybrid Rocket

The hybrid rocket is designed based on the set of formulas given in Section 2.2, and the dimensions of the rocket are as shown in Table 2.

Based on the above dimensions, a 2D geometrical rendering was created, and numerical simulations were conducted to analyze the flow behavior within the combustion chamber (Figure 3).



(**a**) (**b**)

Figure 3. (**a**) Schematic diagram of the hybrid rocket engine; (**b**) the corresponding 3D cross-section image.

Table 2. Dimensions of the hybrid rocket engine.

Parameters	Value	Dimensions
Propellant Design		
Propellant mass	4.249846×10^{-1}	kg
Propellant flow rate	0.042181	kg/s
Fuel design		
Fuel port diameter	0.023175	m
Fuel final diameter	0.050210	m
Fuel length	0.059292	m
Fuel mass	0.084997	kg
Tank design		
Oxidizer mass	0.339988	kg
Tank volume	0.000479	m^3
Tank diameter	0.077494	m
Nozzle design		
Throat diameter	0.006479	m
Exit diameter	0.014487	m
Convergent length	0.008348	m
Divergent length	0.081603	m
Injector design		
Injection area	7.237142×10^{-7}	m^2
Orifice diameter	0.000304	m
Number of holes	10	
Discharge coefficient	0.660000	

The 2D Reynolds-Averaged Navier–Stokes (RANS) simulations were conducted using ANSYS Fluent software 23 R1. The Shear Stress Transport (SST) k-ω turbulence model was selected for its ability to accurately resolve wall-bounded flows, adverse pressure gradients, and heat transfer—critical elements in hybrid rocket simulations. This model provides a robust framework for accurately capturing the near-wall regions, enhancing the predictions of aerodynamic and thermal conditions within the chamber. Furthermore, the Eddy Dissipation Model (EDM) was applied to simulate turbulence-driven combustion; this approach is particularly suitable for diffusion flames, in which combustion is largely governed by turbulent mixing rather than detailed chemical kinetics.

The reaction scheme implemented in this study is described in Equation (11):

$$11C_4H_6 + 95N_2O \Rightarrow 95N_2 + 21CO + 23CO_2 + 28H_2O + 5H_2 \quad (11)$$

3.3. Boundary Conditions

The boundary conditions were a crucial factor in ensuring that the simulations accurately reflected real-world operating conditions. Table 3 presents the specific boundary conditions used in the simulations. The oxidizer temperature is set to 300 K, while the fuel inlet temperature is maintained at 800 K, providing the realistic thermal conditions necessary for the HTPB to pyrolyze and diffuse towards the combustion chamber.

Figure 4 shows the contours of the velocity distribution of the rocket. In the combustion chamber, the velocity remains nearly constant due to the steady-state burning of the propellant. Upon the combustion products entering the nozzle, the velocity consistently increases as the exhaust gases expand and accelerate in response to the pressure-drop within the divergent section. The measured

exhaust velocity was around 1497.418 m/s. Figure 5 shows the corresponding temperature contour within the rocket, revealing the thermal characteristics of the combustion process. The temperature progressively increases along the length of the combustion chamber due to the sustained release of energy from the fuel–oxidizer reactions. The peak temperature of 2231 K is recorded at 0.131473 m from the oxidizer inlet, corresponding to the zone of maximum reaction intensity. The corresponding mass fraction of the fuel can be determined from Figure 6. The mass fraction decreases steadily within the combustion chamber as C_4H_6 is consumed in combustion reactions, releasing energy to sustain the high-temperature conditions. The lowest mass fraction is observed in the nozzle, indicating near-complete utilization of this intermediate species. This trend highlights the efficient combustion within the chamber, which is critical for achieving optimal engine performance and minimizing unburnt residues in the exhaust.

Table 3. Boundary conditions for the numerical simulations for the hybrid rocket.

Mass Flow Rate: Oxidizer (Kg/s)	Mass Flow Rate: Fuel (Kg/s)	Pressure (bar)	Oxidizer Inlet Temperature (K)	Fuel Inlet Temperature (K)
0.03368	0.00842	20	300	800

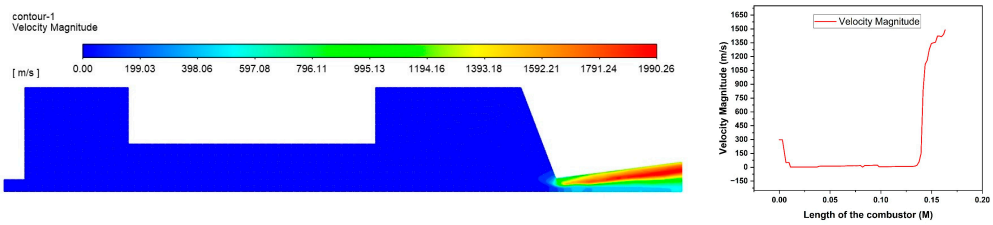


Figure 4. Velocity magnitude inside the hybrid rocket.

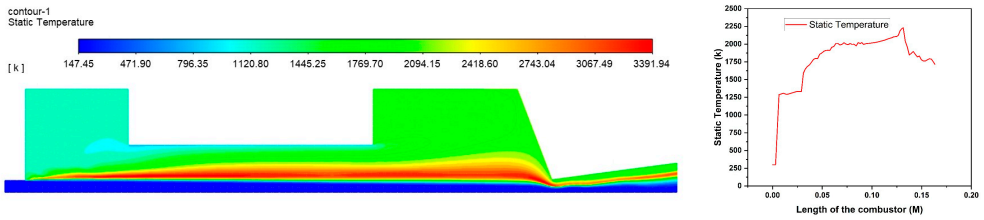


Figure 5. Static temperature inside the hybrid rocket.

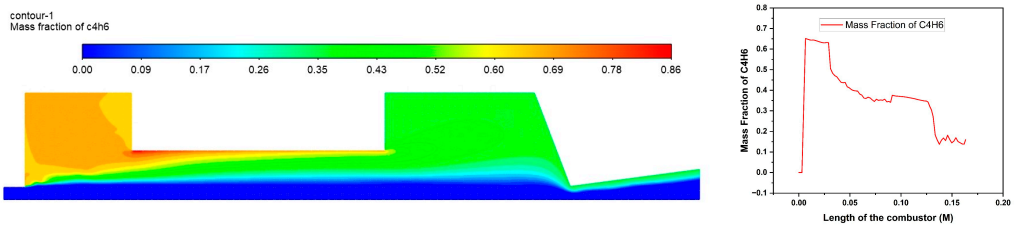


Figure 6. Mass fraction of the C_4H_6 inside the hybrid rocket.

Figure 7 shows the variation in the mass fraction of H_2O along the lengths of the combustion chamber and nozzle. The mass fraction begins increasing from 0.0065 m, corresponding to the initiation of combustion reactions, and reaches its maximum value of 0.070256 at 0.129833 m. Beyond this point, the mass fraction decreases slightly, stabilizing at 0.064268 at the nozzle's exit. This trend reflects the generation of H_2O as a dominant combustion product, providing insights into reaction completeness. The corresponding CO_2 levels can be seen in Figure 8, which shows a consistent increase in the mass fraction of CO_2 extending from the combustion chamber to the nozzle exit. This trend highlights the progressive oxidation of carbon-based species, a key indicator of efficient combustion. At the exhaust, the mass fraction of CO_2 stabilizes at 0.12887, demonstrating the near-complete conversion of the fuel-bound carbon.

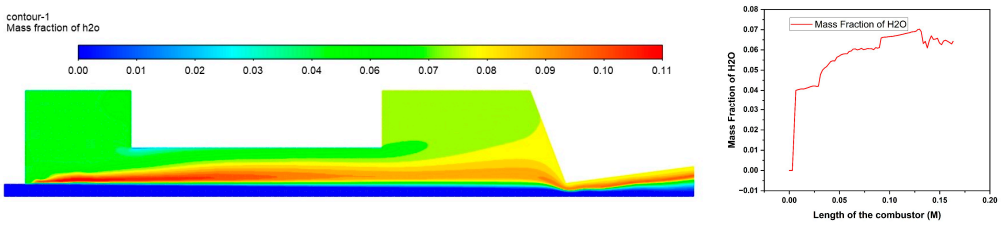


Figure 7. Contours of mass fraction of H_2O inside the hybrid rocket.

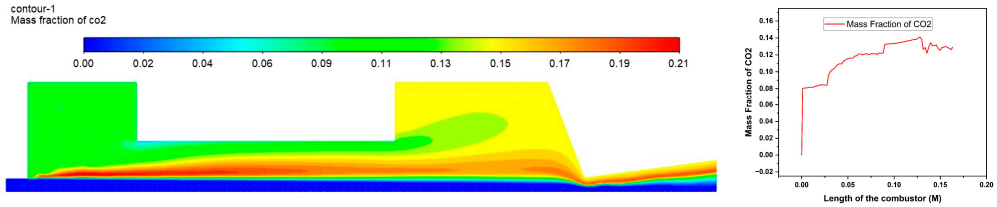


Figure 8. Contours of mass fraction of C_2O inside the hybrid rocket.

4. Conclusions

In the current work, active debris removal methods based on hybrid rocket propulsion were explored. An LEO-based mission at an altitude of 2000 ± 5 km was considered as a target orbit and a 500 km orbit was used as the base orbit for a mothership. The variations of ΔV with respect to Δi and R_f/R_0 have been investigated, and the corresponding energy expenditure determined using the Hohmann transfer. Based on the obtained ΔV, the design, sizing, and numerical modeling of the hybrid rocket engine were performed to determine its potential utilization in the debris removal applications. The mass of the debris that can be handled is limited to 100 kg; the hybrid rocket engine is designed based on this criterion. The whole design could fit in an N Unit CubeSat, along with a mechanical system (such as robotic arm) used to maneuver and handle debris and subsequently deorbit it. The hybrid rocket propulsive module allows for ease in operation in performing both the rendezvous with the selected object and a controlled de-orbiting and atmospheric re-entry. The numerical simulations confirm the potential of hybrid rocket engines for high performance with respect to the mission's applications.

Author Contributions: Conceptualization, S.K.P.; methodology, E.O. and A.I.; software, S.K.P. and A.R.; validation, S.K.P., E.O. and A.I.; formal analysis, S.K.P. and A.R.; investigation, E.O. and A.I.; resources, E.O. and A.I.; data curation, S.K.P. and A.R.; writing—original draft preparation, S.K.P. and A.R.; writing—E.O. and A.I.; visualization, S.K.P.; supervision, E.O. and A.I.; project administration, S.K.P.; funding acquisition, S.K.P. All authors have read and agreed to the published version of the manuscript.

Funding: This research was supported by Italspazio Srl within the 37th cycle of the PON doctoral training program, funded under Grant D.M. No. 1061 of 10 August 2021, as part of its collaboration with the SIA Advanced Space Propulsion Laboratory at the School of Aerospace Engineering—La Sapienza University of Rome.

Institutional Review Board Statement: Not applicable.

Informed Consent Statement: Not applicable.

Data Availability Statement: Data are unavailable due to privacy or ethical restrictions.

Acknowledgments: The authors acknowledge the School of Aerospace—La Sapienza University of Rome.

Conflicts of Interest: Author Sasi Kiran Palateerdham was employed by the company Italspazio srl, Via della Madonnina. The remaining authors declare that the research was conducted in the absence of any commercial or financial relationships that could be construed as a potential conflict of interest.

References

1. Nomura, K.; Rella, S.; Merritt, H.; Baltussen, M.; Bird, D.; Tjuka, A.; Falk, D. Tipping Points of Space Debris in Low Earth Orbit. *Int. J. Commons* **2024**, *18*, 17–31. [CrossRef]
2. Thangavel, K.; Perumal, R.P.; Hussain, K.F.; Gardi, A.; Sabatini, R. Multidisciplinary design and optimization of intelligent Distributed Satellite Systems for EARTH observation. *Acta Astronaut.* **2024**, *216*, 411–427. [CrossRef]
3. Ledkov, A.; Aslanov, V. Review of contact and contactless active space debris removal approaches. *Prog. Aerosp. Sci.* **2022**, *134*, 100858. [CrossRef]
4. Jorgensen, M.K.; Sharf, I. Optimal planning for a multiple space debris removal mission using high accuracy low-thrust transfers. *Acta Astronaut.* **2020**, *172*, 56–69. [CrossRef]
5. Choi, J.H.; Park, C.; Lee, J. Mission planning for active removal of multiple space debris in low Earth orbit. *Adv. Space Res.* **2024**, *73*, 4800–4812. [CrossRef]
6. Mark, C.P.; Kamath, S. Review of Active Space Debris Removal Methods. *Space Policy* **2019**, *47*, 194–206. [CrossRef]
7. Kessler, D.J.; Johnson, N.L.; Liou, J.C.; Matney, M. The kessler syndrome: Implications to future space Operations. *Adv. Astronaut. Sci.* **2010**, *137*, 2010.
8. Kessler, D.J.; Cour-Palais, B.G. Collision frequency of artificial satellites: The creation of a debris belt. *J. Geophys. Res.* **1978**, *83*, 2637–2646. [CrossRef]
9. AIAA Technical Committee on Space Systems. *Space Debris: An AIAA Position Paper*; American Institute of Aeronautics and Astronautics (AIAA): Reston, VA, USA, 1981.
10. European Space Agency, ESA Space Debris Working Group. *Space Debris: The Report of the ESA Space Debris Working Group (SDWG), ESA SP-1109*; European Space Agency: Paris, France, 1988.
11. Benkö, M.; Schrogl, K.-U. (Eds.) The 1999 UNCOPUOS "Technical Report on Space Debris" and the New Work Plan on Space Debris (2002–2005): Perspectives and legal consequences. In Proceedings of the Third European Conference on Space Debris, Darmstadt, Germany, 19–21 March 2001; ESA Publications Division: Noordwijk, The Netherlands, 2001; Volume 2.
12. International Academy of Astronautics (IAA). *IAA Space Debris Subcommittee, Position Paper on Orbital Debris*; International Academy of Astronautics (IAA): Paris, France, 2001.
13. Inter-Agency Space Debris Coordination Committee (IADC). (n.d.) Available online: https://www.iadc-home.org/what_iadc (accessed on 11 October 2024).
14. Inter-Agency Space Debris Coordination Committee (IADC); IADC Steering Group & Working Group 4. *Space Debris Mitigation Guide- lines, IADC-02-01, Rev. 1 Edition*; Issued by IADC Steering Group and Working Group: Berlin, Germany, 2007.
15. DeLuca, L.; Bernelli, F.; Maggi, F.; Tadini, P.; Pardini, C.; Anselmo, L.; Grassi, M.; Pavarin, D.; Francesconi, A.; Branz, F.; et al. Active space debris removal by a hybrid propulsion module. *Acta Astronaut.* **2013**, *91*, 20–33. [CrossRef]
16. Hakima, H.; Bazzocchi, M.C.; Emami, M.R. A deorbiter CubeSat for active orbital debris removal. *Adv. Space Res.* **2018**, *61*, 2377–2392. [CrossRef]
17. Barbee, B.W.; Alfano, S.; Pinon, E.; Gold, K.; Gaylor, D. Design of Spacecraft Missions to Remove Multiple Orbital Debris Objects. In Proceedings of the 35th Annual Aas Guidance and Control Conference, Breckenridge, Colorado, 3–8 February 2012; AAS Publications: Washington, DC, USA, 2012; pp. 93–110.
18. Udrea, B.; Nayak, M. A cooperative multi-satellite mission for controlled active debris removal from low Earth orbit. In Proceedings of the IEEE Aerospace Conference, Big Sky, MT, USA, 7–14 March 2015; pp. 1–15. [CrossRef]
19. Nishida, S.; Kawamoto, S.; Okawa, Y.; Terui, F.; Kitamura, S. Space debris removal system using a small satellite. *Acta Astronaut.* **2009**, *65*, 95–102. [CrossRef]
20. Castronuovo, M.M. Active space debris removal—A preliminary mission analysis and design. *Acta Astronaut.* **2011**, *69*, 848–859. [CrossRef]
21. Tadini, P.; Tancredi, U.; Grassi, M.; Anselmo, L.; Pardini, C.; Francesconi, A.; Branz, F.; Maggi, F.; Lavagna, M.; DeLuca, L.; et al. Active debris multi-removal mission concept based on hybrid propulsion. *Acta Astronaut.* **2014**, *103*, 26–35. [CrossRef]
22. Bate, R.R.; Mueller, D.D.; White, J.E. *Fundamentals of Astrodynamics*; Courier Dover Publications: Garden City, NY, USA, 1971.

23. Rocket Propulsion Elements–Eighth edition G. P. Sutton and O. Biblarz John Wiley and Sons, The Atrium, Southern Gate, Chichester, West Sussex, PO19 8SQ, UK, 2010. 768pp. Illustrated. £90. ISBN 978-0-470-08024-5. *Aeronaut. J.* **2011**, *115*, 65. Available online: https://www.cambridge.org/core/journals/aeronautical-journal/article/abs/rocket-propulsion-elements-eighth-edition-g-p-sutton-and-o-biblarz-john-wiley-and-sons-the-atrium-southern-gate-chichester-west-sussex-po19-8sq-uk-2010-768pp-illustrated-90-isbn-9780470080245/2A715CD2A292E67325345307C655C839 (accessed on 11 October 2024). [CrossRef]
24. Srivastava, S.; Ingenito, A.; Andriani, R. Numerical and Experimental Study of a 200 N Paraffin/N_2O hybrid rocket. In Proceedings of the EUCASS 2019-8th European Conference for Aeronautics and Space Sciences, Madrid, Spain, 1–4 July 2019.

Disclaimer/Publisher's Note: The statements, opinions and data contained in all publications are solely those of the individual author(s) and contributor(s) and not of MDPI and/or the editor(s). MDPI and/or the editor(s) disclaim responsibility for any injury to people or property resulting from any ideas, methods, instructions or products referred to in the content.